Inactivation of the microRNA-*183/96/182* cluster results in syndromic retinal degeneration

Stephen Lumayag[a,b,c], Caroline E. Haldin[a,b,c], Nicola J. Corbett[c], Karl J. Wahlin[d], Colleen Cowan[a,b,c], Sanja Turturro[a,b,c], Peter E. Larsen[e], Beatrix Kovacs[a,b,c], P. Dane Witmer[f], David Valle[f], Donald J. Zack[d], Daniel A. Nicholson[c], and Shunbin Xu[a,b,c,1]

Departments of [a]Pharmacology, [b]Ophthalmology, and [c]Neurological Sciences, Rush University Medical Center, Chicago, IL 60612; [d]Wilmer Eye Institute, The Johns Hopkins University School of Medicine, Baltimore, MD 21287; [e]Biosciences Division, Argonne National Laboratory, Lemont, IL 60439; and [f]McKusick-Nathans Institute of Genetic Medicine, The Johns Hopkins University School of Medicine, Baltimore, MD 21205

Edited by Jeremy Nathans, The Johns Hopkins University, Baltimore, MD, and approved December 21, 2012 (received for review July 31, 2012)

The microRNA-*183/96/182* cluster is highly expressed in the retina and other sensory organs. To uncover its in vivo functions in the retina, we generated a knockout mouse model, designated "*miR-183C*$^{GT/GT}$," using a gene-trap embryonic stem cell clone. We provide evidence that inactivation of the cluster results in early-onset and progressive synaptic defects of the photoreceptors, leading to abnormalities of scotopic and photopic electroretinograms with decreased *b*-wave amplitude as the primary defect and progressive retinal degeneration. In addition, inactivation of the *miR-183/96/182* cluster resulted in global changes in retinal gene expression, with enrichment of genes important for synaptogenesis, synaptic transmission, photoreceptor morphogenesis, and phototransduction, suggesting that the *miR-183/96/182* cluster plays important roles in postnatal functional differentiation and synaptic connectivity of photoreceptors.

MicroRNAs (miRNAs) are small, endogenous, noncoding, regulatory RNAs and represent a newly recognized level of gene-expression regulation (1–4). miRNAs have unique expression profiles in the developing and adult retina and are involved in normal development and functions of the retina in all species studied so far (5–12). miRNAs are dysregulated in the retina of retinal degenerative mouse models, suggesting their potential involvement in retinal degeneration (13, 14). Conditional inactivation of dicer, an RNase III endonuclease required for miRNA maturation in cytosol (15), in the mouse retina resulted in alteration of retinal differentiation and optic-cup patterning, increased cell death, and disorganization of axons of retinal ganglion cells (16–19), suggesting that miRNAs are important for normal development and functions of the mammalian retina. However, in vivo functions of individual miRNAs in the retina still are largely unknown.

Previously, we identified a highly conserved, intergenic, sensory organ-specific, paralogous miRNA cluster, the *miR-183/96/182* cluster (hereafter, *miR-183/96/182*), contained within an ∼4-kb genomic segment on mouse chr6qA3.3 (8, 9). In the adult retina, *miR-183/96/182* is expressed specifically in all photoreceptors and in the inner nuclear layer (8, 10). Developmentally, its expression is minimal in the embryonic retina but increases dramatically after birth and peaks in the adult retina, suggesting a role for *miR-183/96/182* in maturation and normal functioning of the adult retina (8, 9). Additionally, expression of *miR-183/96/182* has a diurnal pattern, suggesting a potential role in rhythmic functions of the retina (8, 9). Recently, *miR-183/96/182* also was shown to be light responsive, independent of the circadian cycle (20). Targeted deletion of *miR-182* alone in mouse did not result in a discernible phenotype, suggesting functional compensation by *miR-183* and *miR-96* (21). Point mutations of *miR-96* were reported to result in progressive, nonsyndromic hearing loss in both human (22) and mouse (23); however, there was no apparent retinal phenotype, an observation that suggests *miR-96* plays a major role in the inner ear but not in the retina (22–25). Finally, a recent report showed that knockdown of *miR-183/96/182* in postmitotic rod photoreceptors in a miRNA-sponge transgenic mouse model resulted in increased susceptibility to light damage in the retina (26); however, no histological or functional defects of the retina were observed under normal lighting conditions (26). Thus, in vivo functions of *miR-183/96/182* in the retina remain uncertain.

To search for the in vivo functions of *miR-183/96/182*, we first dissected the genomic structure of the gene encoding *miR-183/96/182* (hereafter referred to as "the *miR-183/96/182* gene") and characterized a gene-trap embryonic stem cell (ESC) clone (27–29) in which the gene-trap construct was inserted downstream of the first exon of the *miR-183/96/182* gene, designated as "*miR-183C*^{GT} allele." Using this ESC clone, we generated a mouse model, designated as "*miR-183C*$^{GT/GT}$," in which the *miR-183/96/182* gene is inactivated, and the β-geo cassette in the gene-trap construct reliably mirrors the endogenous expression patterns of *miR-183/96/182*.

Results

***miR-183/96/182* Cluster Resides in the Intron of a Potentially Protein-Coding Gene.** The genomic features around *miR-183/96/182* include two CpG islands ∼3.4–6.5 kb 5′ of *premiR-183*, the most 5′ miRNA of the cluster (Fig. 1*A*; and *SI Appendix*, Fig. S1 and Sequence (Seq.) S1) (http://genome.UCSC.edu/) (8). A cDNA clone, AK044220, extends ∼3.2–4.6 kb 5′ to *premiR-183*, encompassing the second CpG island (Fig. 1*A* and *SI Appendix*, Fig. S1). Multiple expressed sequences detected in gene-trap clones (27), including D016D06 (28, 29) [deposited by the German GeneTrap Consortium (GGTC) (http://tikus.gsf.de)], colocalize in AK044220 (Fig. 1*A* and *SI Appendix*, Fig. S1), suggesting a 5′ exon of the *miR-183/96/182* gene. The region 3′ of *miR-183/96/182* contains an EST clone, BB709579, ∼6 kb 3′ of *premiR-182* (Fig. 1*A*), suggesting the *miR-183/96/182* gene has a downstream exon. To confirm this model, we designed multiple primers complementary to the predicted exons to perform 5′ and 3′ RACE and RT-PCR using total RNA of the mouse retina and D016D06 ESCs followed by sequencing (see *SI Appendix*, Figs. S2 and S3 for details).

Our results showed that the *miR-183/96/182* gene spans more than 15 kb, with at least two alternatively spliced transcripts (Fig. 1*B*). Both transcripts start from the nucleotide (nt) G, 3,943 nt 5′ to *premiR-183* (−3943G) and use the same exon 1 (Ex1) (Fig. 1*B* and *SI Appendix*, Seq. S1). Transcript I is at least 979 nt and comprises Ex1 and exon 2 (Ex2), separated by a 3,213-bp intron. However, the 3′ RACE product detecting Ex2 stopped 197 nt 5′ to *premiR-183* and did not extend beyond *miR-183/96/182* (Fig. 1*B* and *SI Appendix*, Seq. S1). Thus, the 3′ end of transcript I is not yet fully determined. Transcript II is about 1,432 nt and consists of Ex1 and

Author contributions: D.V., D.J.Z., D.A.N., and S.X. designed research; S.L., C.E.H., N.J.C., K.J.W., C.C., S.T., B.K., P.D.W., D.A.N., and S.X. performed research; S.L., C.E.H., N.J.C., K.J.W., C.C., P.E.L., D.A.N., and S.X. analyzed data; and S.X. wrote the paper.

The authors declare no conflict of interest.

This article is a PNAS Direct Submission.

Data deposition: The sequences reported in this paper have been deposited in the GenBank database (accession nos. KC408930 and KC408931).

[1]To whom correspondence should be addressed. E-mail: shunbin_xu@rush.edu.

See Author Summary on page 1990 (volume 110, number 6).

This article contains supporting information online at www.pnas.org/lookup/suppl/doi:10.1073/pnas.1212655110/-/DCSupplemental.

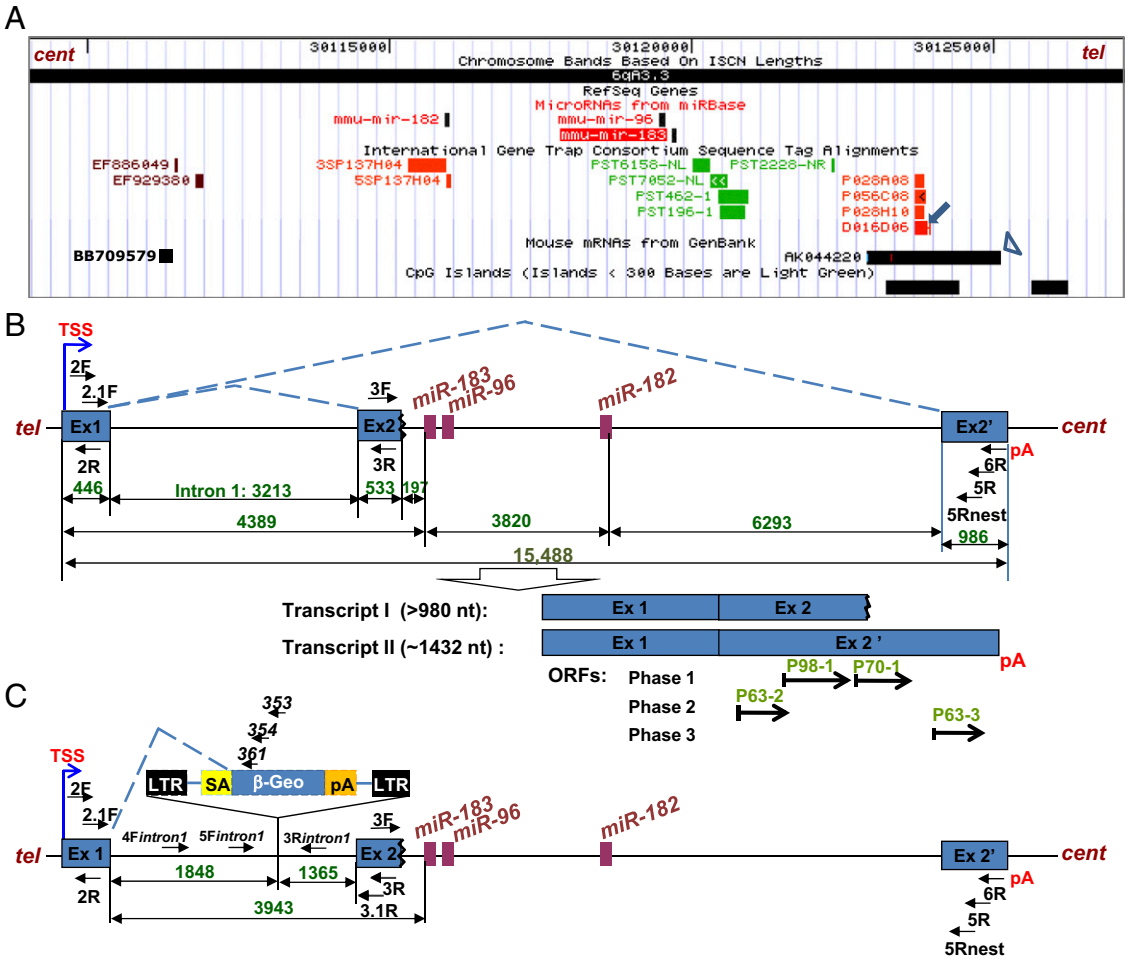

Fig. 1. Genomic structures of the *miR-183/96/182* gene and the *miR-183C*^{GT} allele of the gene-trap cell line D016D06. (*A*) Genomic features around the *miR-183/96/182* gene compiled from the University of California, Santa Cruz Genome Browser (Mouse July 2007 Assembly). The blue arrow points to the gene-trap clone, D016D06. The open arrowhead points to the mouse cDNA clone, AK044220. *tel*, telomeric; *cent*, centromeric. (*B*) Genomic structure of the *miR-183/96/182* gene. Blue boxes represent exons. The dotted blue lines indicate splicing events. pA, polyA signal. One-headed arrows mark locations and directions of exonic primers 2F, 2.1F, 3F, 3R, 5R, 5Rnest, and 6R. The numbers above the double-headed arrows denote the distances (in bp) between the vertical lines. The wavy end of Ex2 indicates that the 3′ end of this exon not yet fully defined. Alternative splicing events result in two forms of transcripts, transcripts I and II. Transcript II has four putative ORFs. In phase I of the sequence, two ORFs consist of 98 (P98-1) and 70 (P70-1) codons, respectively. Phases 2 and 3 each have an ORF of 63 codons (P63-2 and P63-3). (*C*) Genomic structure of the *miR-183C*^{GT} allele of the gene-trap clone D016D06. The gene-trap construct was inserted in intron 1 of the *miR-183/96/182* gene. Location and directions of primers, 4Fintron1, 5Fintron1, *353, 354,* and *361* are labeled. LTR, long tandem repeat.

an alternatively spliced exon 2′ (Ex2′), which is 14 kb downstream of Ex1. Ex2′ is 986 bp in size with a polyA signal (Fig. 1*B* and *SI Appendix*, Seq. S1). The structure of transcript II clearly positions *miR-183/96/182* in the intron of the *miR-183/96/182* gene (Fig. 1*B* and *SI Appendix*, Seq. S1).

Transcript I has no ORF >30 codons, whereas transcript II has at least four ORFs, all of which reside in Ex 2′ (Fig. 1*B* and *SI Appendix*, Seqs. S2 and S3). In phase I of the sequence, two ORFs consist of 98 (P98-1) and 70 (P70-1) codons, respectively. Phases 2 and 3 each have an ORF of 63 codons (P63-2 and P63-3). None of the putative peptides contain known conserved functional domains; however, P98-1 encodes motifs found in proteins from multiple species (*SI Appendix*, Fig. S4). Thus, there is a possibility that the *miR-183/96/182* gene encodes one or more peptides.

Characterization of the Gene-Trap Allele, *miR-183C*^{GT}, and Production of *miR-183C*$^{GT/GT}$ Mice. Gene-trap clone D016D06 was derived from insertion of a retroviral construct, rFlpROSAβgeo, in 129S2 ESCs (Fig. 1 *A* and *C*) (http://tikus.gsf.de) (28, 29). The rFlpROSAβgeo construct carries a promoterless reporter gene, the β-geo cassette [an in-frame fusion of the β-galactosidase and neomycin resistance genes (30)], with a splicing acceptor (SA) immediately upstream and a polyA signal downstream of the β-geo cassette (Fig. 1*C*). To determine the location of the insertion of the construct in the "gene-trapped" allele, designated as "*miR-183C*^{GT}," we sequenced the product of genomic PCR using primers in intron 1 and in the gene-trap construct (Fig. 1*C* and *SI Appendix*, Seq. S1). Our results revealed that the gene-trap construct was inserted 1,848 bp downstream of Ex1 in intron 1 of the *miR-183/96/182* gene. In the trapped allele, Ex1 of *miR-183/96/182* gene spliced to β-geo, creating a fusion transcript (Fig. 1*C*) that stops after the polyA signal of the β-geo cassette, preventing transcription of *miR-183/96/182*. This result predicts that *miR-183C*$^{GT/GT}$ mice would have complete loss of function of the *miR-183/96/182* gene, whereas the β-geo cassette under the control of native regulatory elements should report endogenous expression pattern of the gene.

To test this model, we generated chimeric mice using the D016D06 ESCs (*SI Appendix*, Figs. S5–S7 and Table S1). Germline-transmitting F1 and F2 mice were produced. Genotypes of the F2 mice followed the expected Mendelian inheritance pattern (*SI Appendix*, Fig. S8). The *miR-183C*$^{GT/GT}$ mice generally had decreased body weight (by ~24%) and size (*SI Appendix*, Fig. S8);

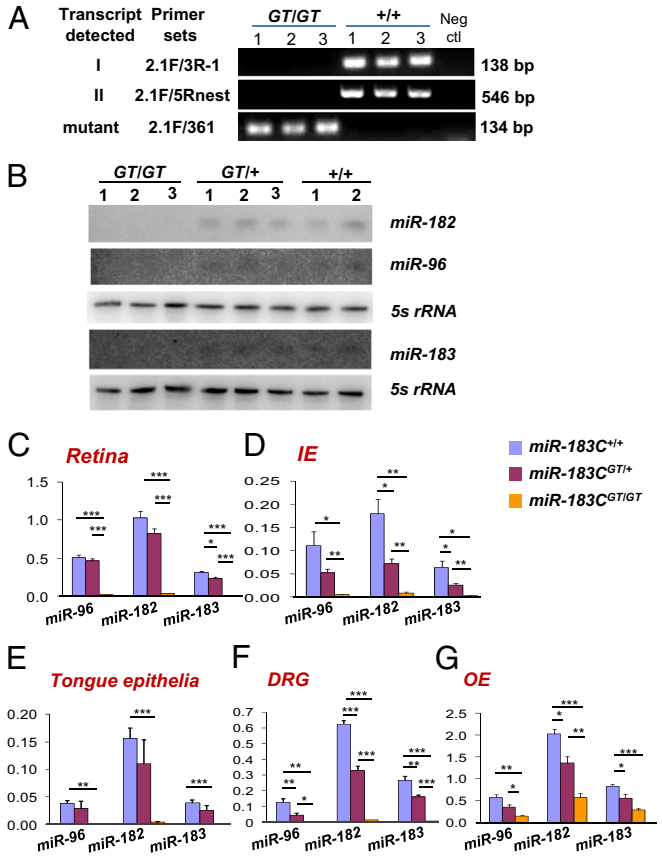

Fig. 2. The *miR-183/96/182* gene is inactivated in the retina and other sensory organs of *miR-183C*$^{GT/GT}$ mice. (*A*) RT-PCR analysis of the transcripts of the *miR-183/96/182* gene and the fusion transcript of the *miR-183C*^{GT} allele. Transcript I was detected by RT-PCR using primers 2F/3R followed by nested PCR using 2.1F/3R-1. Transcript II was detected by RT-PCR using 2F/5R and nested PCR using 2.1F/5Rnest. The Ex1/β-geo fusion transcript of the *miR-183C*^{GT} allele was detected by RT-PCR with primers 2F/254 and nested PCR with 2.1F/361. (*B*) Northern blot analysis. (*C*–*G*) qRT-PCR analysis of the expression of members of the *miR-183/96/182* cluster in the retina (*C*), IE (*D*), tongue epithelia (*E*), DRG (*F*), and OE (*G*). $*P < 0.05$; $**P < 0.01$; $***P < 0.001$. *miR-183C*$^{+/+}$: $n = 4$; *miR-183C*$^{GT/+}$: $n = 4$ (6 for DRG); *miR-183C*$^{GT/GT}$: $n = 3$ (4 for DRG).

however, their overall survival and life span were not significantly different from their wild-type and heterozygous littermates.

***miR-183/96/182* Gene Is Inactivated in the Retina and All Sensory Organs of *miR-183C*$^{GT/GT}$ Mice.** Using RT-PCR (Fig. 2 *A* and *C*) and Northern blot analyses (Fig. 2*B*), we showed that both alternatively spliced transcripts (Fig. 2*A*) and three mature miRNAs of the *miR-183/96/182* gene were undetectable in the retina of *miR-183C*$^{GT/GT}$ mice (Fig. 2 *B* and *C*), whereas the Ex1/β-geo fusion transcript was present only in *miR-183C*$^{GT/GT}$ but not in the wild-type retina (Fig. 2*A*). Similarly, all *3p* miRNAs of the cluster also were abolished in the retina (*SI Appendix*, Fig. S9*B*).

To test whether the expression of *miR-183/96/182* was affected in other sensory organs, we performed quantitative RT-PCR (qRT-PCR) analysis using RNA isolated from the inner ear (IE), tongue epithelia, dorsal root ganglions (DRGs), and olfactory epithelia (OE) (Fig. 2 *D*–*G*) and found no detectable expression of *miR-183/96/182* in any major sensory organs of *miR-183C*$^{GT/GT}$ mice.

We conclude that the *miR-183/96/182* gene was completely inactivated in *miR-183C*$^{GT/GT}$ mice.

β-Geo Cassette Reports Endogenous Expression Patterns of the *miR-183/96/182* Gene. X-Gal staining in the adult *miR-183C*$^{GT/+}$ retina showed specific expression of β-gal in all photoreceptors in the outer nuclear layer (ONL) and in a subgroup of ganglion cells (Fig. 3 *A*–*C*), similar to the previously described expression pattern of *miR-183/96/182* (5, 8–10). We also observed staining in the outer portion of the inner nuclear layer (INL); the punctate pattern suggested that the X-gal positive signals in the INL possibly were derived from synapses of the photoreceptors (*SI Appendix*, Fig. S10).

X-Gal staining of retina harvested every 4 h from adult *miR-183C*$^{GT/+}$ mice maintained in constant darkness showed that the intensity of X-Gal staining in photoreceptors followed a circadian rhythm, with peak intensity at Circadian Time (CT)1 and trough at CT13 (Fig. 3 *D* and *E*). This rhythm is in an approximately opposite phase to that we detected for *miR-183/96/182* at the RNA level (8), likely reflecting the delay from transcription to the production of functional β-gal protein. Similar delays from transcription to protein expression have been reported in many other rhythmic genes (31–33).

To demonstrate the developmental expression pattern, we performed X-Gal staining in the retinas of embryonic day (E)10.5, E14.5, E16.5, and E18.5 and postnatal day (P)1, P2, P5, and P10 heterozygous mice. The result showed that, similar to our previous qRT-PCR analysis on the mature miRNAs of the cluster (8), β-gal was not detectable in the embryonic stages or at P1 but started to express in the outer neuroblast layer (ONBL) at P2, was drastically up-regulated at P5, and was increased further at P10 and the adult stage (Fig. 3*F*). We conclude that the β-geo cassette of the *miR-183C*^{GT} allele reports the endogenous expression pattern of the *miR-183/96/182* gene in the retina developmentally, spatially, and temporally.

Also consistent with our previous results at the RNA level, X-Gal staining in other sensory organs of *miR-183C*$^{GT/+}$ mice showed specific expression in all sensory epithelia in the IE, OE, and the pheromone-sensing vomeronasal organ (VNO), papillae of tongue epithelia, and DRGs (Fig. 4; and *SI Appendix*, Figs. S11–S13). We also observed abundant expression in the olfactory bulbs (Fig. 4 *C*, *a* and *SI Appendix*, Fig. S14), possibly as a result of the expression in the axons and synaptic terminals of receptor neurons in the OE and VNO. Like many other retina-specific genes (34, 35), the *miR-183/96/182* gene also is expressed in the pineal body (Fig. 4 *C*, *b* and *SI Appendix*, Fig. S14).

Inactivation of the *miR-183/96/182* Gene Results in Functional Defects in the Retina. To assess retinal function, we performed scotopic (Fig. 5 *A* and *B*) and photopic (Fig. 5 *C* and *D*) electroretinograms (ERGs) on 5-wk-, 6-mo-, and 1-y-old *miR-183C*$^{GT/GT}$ mice. The most prominent defect, decreased *b*-wave amplitude in *miR-183C*$^{GT/GT}$ mice as compared with their age-matched, wild-type controls, was common to scotopic (Fig. 5 *B*, *g*–*i*) and photopic ERGs (Fig. 5*D*) and was detectable in mice as early as 5 wk of age, at a time when the histology of the retina was normal (see below). The ERG abnormalities progressed with age, and photopic *b*-wave amplitudes were more severely affected than scotopic ERGs (Fig. 5 and *SI Appendix*, Fig. S15 and Table S2). At 1 y of age, the photopic *b*-wave amplitude of *miR-183C*$^{GT/GT}$ mice was <10% that of wild-type littermate controls (Fig. 5*D*). The ERG *b* wave is derived mostly from activities of depolarizing bipolar cells (36–39); defects in bipolar cells and photoreceptor synaptic transmission can produce defective *b* waves. Because *miR-183/96/182* is expressed predominantly in photoreceptors, it is likely that the reduction in *b*-wave amplitude in *miR-183C*$^{GT/GT}$ mice reflects defective synaptic transmission in rods and cones.

The photopic and scotopic *a*-wave amplitudes were normal in 5-wk-old *miR-183C*$^{GT/GT}$ mice but decreased with age, and, as with the *b* wave, the photopic amplitude decreased more quickly than the scotopic amplitude (Fig. 5 *B*, *a*–*c* and *D*): At 6 mo of age the photopic *a*-wave amplitude was reduced to 40% of control, and by 1 y it was <10% of control. The scotopic *a*-wave amplitude was normal until age 1 y, when it was reduced to 43–65% of control (Fig. 5*D* and *SI Appendix*, Table S2). The ERG *a* wave reflects the electrical response of photoreceptors to light (40–42). These results suggest that in *miR-183C*$^{GT/GT}$ mice the phototransduction pathways of rods and cones became significantly compromised with time, cones more so than rods.

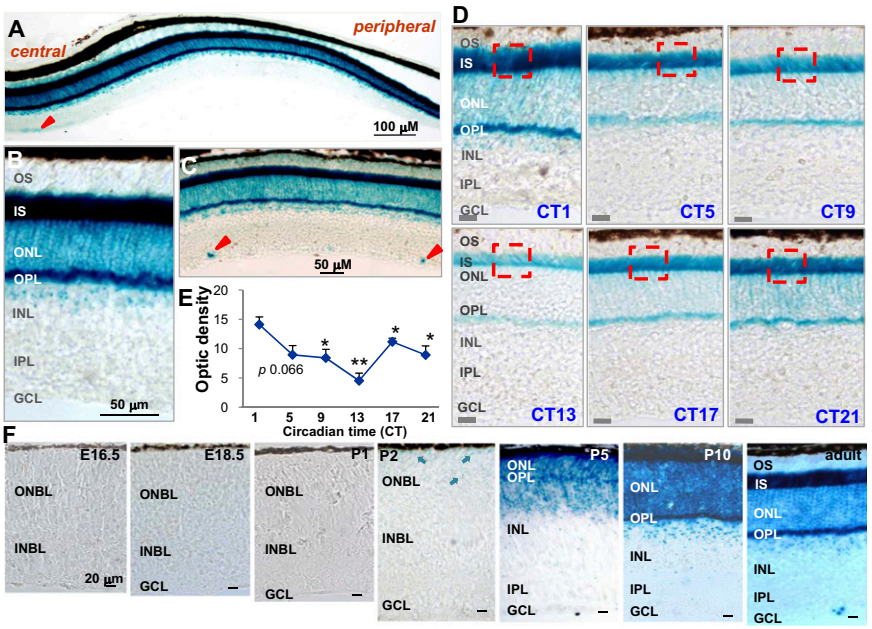

Fig. 3. Expression of the β-geo cassette reflects the endogenous expression patterns of the *miR-183/96/182* gene in the retina. (*A*–*C*) X-Gal staining of the retina. Red arrowheads in *A* and *C* show the expression in a subgroup of ganglion cells. OS, outer segment; IS, inner segment; IPL, inner plexiform layer; GCL, ganglion cell layer. (*D*) Expression of the β-geo cassette in photoreceptors of *miR-183C*$^{GT/+}$ mice has a circadian rhythm. X-Gal staining of retinal sections of *miR-183C*$^{GT/+}$ mice harvested every 4 h in a circadian cycle. (Scale bar: 20 μm.) Red dotted lines indicate unit squares used to measure optic density shown in *E*. (*E*) Relative optic density of X-Gal signals in the inner segment of photoreceptors in a unit square (illustrated in *D*). $n = 3$ at all time points. $^{*}P < 0.05$; $^{**}P < 0.01$ compared with CT1. (*F*) X-Gal staining of the retina of E14.5, E16.5, E18.5, P1, P2, P5, P10, and adult *miR-183C*$^{GT/+}$ mice. Arrows in P2 indicate positive signals in the outer neuroblast layer. The OPL started to form at P5. At this stage, ~40% of photoreceptors are still in the INL (115) and are positive to X-Gal staining. INBL, inner neuroblast layer.

ERG latency, the time from the onset of stimulus to the beginning of the *a* wave, and implicit time, the time from the onset of light stimulus to the peak of the *b* wave, of both scotopic and photopic ERGs were increased in *miR-183C*$^{GT/GT}$ mice from age 6 mo, with more severe and persistent changes in photopic ERGs (Fig. 5 *B* and *D* and *SI Appendix*, Table S2), suggesting more severe synaptic transmission defects in the cone pathway.

ERG tests in heterozygous *miR-183C*$^{+/GT}$ mice at all ages showed no significant defects compared with their age-matched wild-type controls.

Inactivation of the *miR-183/96/182* Gene Results in Progressive Retinal Degeneration. At 5 wk of age, despite significant ERG abnormalities, the retinas of *miR-183C*$^{GT/GT}$ mice were histologically indistinguishable from those of littermate controls (Fig. 6*A*). By age 6 mo, however, *miR-183C*$^{GT/GT}$ mice showed retinal degeneration with decreased thickness of the ONL (Fig. 6*B*), which had progressed at 1 y of age (Fig. 6*C*). Intriguingly, the superior retina was more affected than the inferior retina. At age 6 mo, the number of nuclear layers of the ONL of the superior retina was decreased by ~30%, whereas no significant changes were detected in the inferior retina (Fig. 6*B*). At age 1 y, ONL thickness was decreased in the entire eye, but the superior retina continued to be affected more severely (decreased by 40–52%) than the inferior retina (decreased by 30–43%) (Fig. 6*C*).

Consistent with ERG results, heterozygous *miR-183C*$^{+/GT}$ mice showed no significant retinal degeneration compared with wild-type littermates at all ages tested.

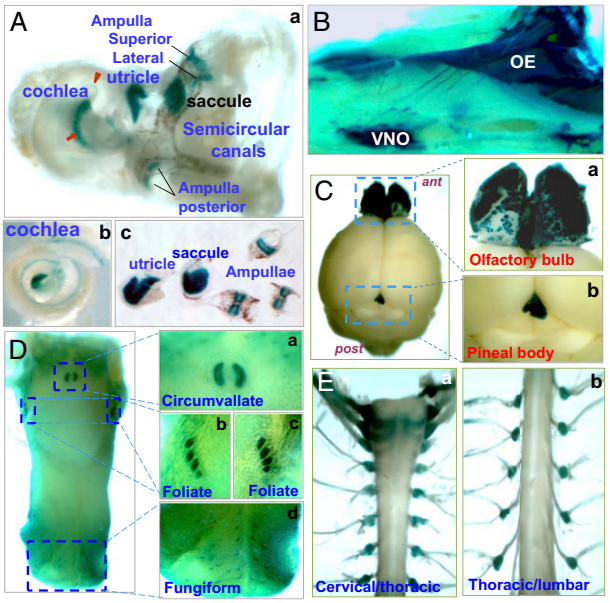

Fig. 4. Expression of the β-geo cassette reflects the endogenous expression pattern of the *miR-183/96/182* cluster in other sensory and related organs. X-Gal staining of the IE (*A* a–c), OE and VNO (*B*), OB (*C a*), pineal body (*C b*), papillae of the tongue (*D a*–*d*), and DRG (*E a* and *b*) of adult *miR-183C*$^{GT/+}$ mice.

Inactivation of the *miR-183/96/182* Gene Results in Increased Susceptibility to Light Damage. To determine if *miR-183/96/182* influences the response of the retina to light damage, we exposed *miR-183C*$^{GT/GT}$ mice and wild-type littermates to 10,000-lx cool, white fluorescent light for 2 h followed by 2 wk in the dark. Retinas of *miR-183C*$^{GT/GT}$ mice showed increased light toxicity as compared with wild-type littermates (Fig. 6*D* and *SI Appendix*, Fig. S16). As with aging, the superior retina was more damaged than the inferior retina. The number of nuclear layers in ONL of the superior retina was decreased by 48–62% in *miR-183C*$^{GT/GT}$ mice compared with their wild-type littermates; this decrease was similar to or worse than the extent of degeneration in 1-y-old *miR-183C*$^{GT/GT}$ mice without light exposure (Fig. 6 *C* and *D*). The inferior retina had much less damage, suggesting that the superior retina is intrinsically more vulnerable to degenerative changes. This result is consistent with a recent report that knockdown of *miR-183/96/182* in postmitotic photoreceptors resulted in increased susceptibility to light damage in the superior but not the inferior retina (26).

Inactivation of the *miR-183/96/182* Gene Results in Photoreceptor Ribbon Synaptic Defects. To identify target genes of *miR-183/96/182* and to understand the mechanisms of functional defects in the retina of *miR-183C*$^{GT/GT}$ mice, we performed gene-expression profiling using the Affymetrix GeneChip Mouse Genome 430A_2.0 and total RNA from 5-wk-old *miR-183C*$^{GT/GT}$ mice, a time when there is no histological evidence of degeneration in the retina (*SI Appendix*, Fig. S17 and Tables S3–S9). A total of

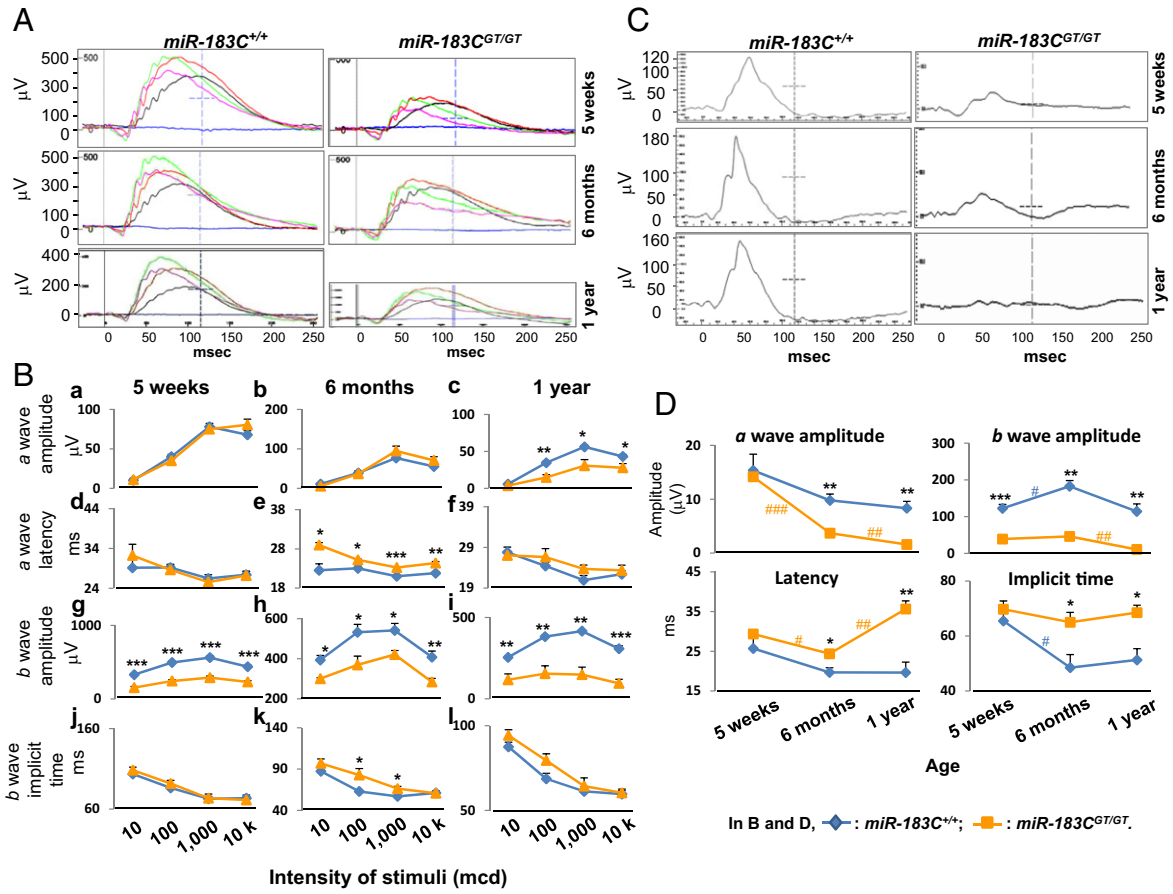

Fig. 5. Inactivation of the *miR-183/96/182* gene resulted in progressive ERG defects. (*A* and *C*) Representative scotopic (*A*) and photopic (*C*) ERG recordings of 5-wk-, 6-mo-, and 1-y-old mice. In *A*, blue, black, red, green, and violet lines represent recordings at 0, 10, 100, 1 k, and 10 k mcd·s·m^{-2}, respectively. (*B*) Comparison of scotopic *a*- and *b*-wave amplitudes, latency, and implicit time of *miR-183C*$^{GT/GT}$ and age-matched wild-type control mice. *miR-183C*$^{+/+}$: n = 12, 4, and 4 for 5-wk- (*a*, *d*, *g*, *j*), 6-mo- (*b*, *e*, *h*, *k*), and 1-y-old (*c*, *f*, *i*, *l*) mice, respectively; *miR-183C*$^{GT/GT}$: n = 10, 3, and 4 for 5-wk-, 6-mo-, and 1-y-old mice, respectively. $^{*}P < 0.05$; $^{**}P < 0.01$; $^{***}P < 0.001$ between *miR-183C*$^{GT/GT}$ and age-matched wild-type controls. (*D*) Comparison of photopic *a*- and *b*-wave amplitudes, latency and implicit time of *miR-183C*$^{GT/GT}$ and age-matched wild-type control mice. *miR-183C*$^{+/+}$: n = 3 at all ages; *miR-183C*$^{GT/GT}$: n = 4, 3, and 4 for 5-wk-, 6-mo-, and 1-y-old mice, respectively. Error bars indicate SEM. $^{\#}P < 0.05$; $^{\#\#}P < 0.01$; $^{\#\#\#}P < 0.001$ between two age groups.

1,341 genes showed significant differences in expression levels in *miR-183C*$^{GT/GT}$ mice as compared with wild-type littermates ($P < 0.05$; fold change ≥1.2 folds) (*SI Appendix*, Tables S4–S6). Functional annotation analysis of the genes with altered expression showed significant enrichment for those involved in synaptogenesis ($P = 3.2 \times 10^{-3}$), synaptic contact ($P = 3.9 \times 10^{-3}$), and transmission of nerve impulses ($P = 6.8 \times 10^{-3}$) (*SI Appendix*, Table S7 *A* and *B*). In addition, key members of the classical complement system and Class I MHC (MHCI) molecules also were significantly enriched in the genes with increased expression (*SI Appendix*, Table S8). Members of the classical complement cascade and MHCI are expressed in retina and the central nervous system and play important roles in synaptic remodeling and connectivity (43–49). These results are consistent with the ERG data indicating that inactivation of *miR-183/96/182* gene results in abnormal photoreceptor synaptic transmission.

Neurotransmission of retinal photoreceptors is accomplished by a unique type of chemical synapse—the ribbon synapse—at their termini (50, 51). To evaluate the status of photoreceptor termini and ribbon synapses, we first performed immunofluorescence (IF) using synaptic markers. Ribeye/CtBP2, a major component of synaptic ribbons (52), normally has a horseshoe-shaped staining pattern in the wild-type photoreceptor termini (Fig. 7 *A* and *C*). However, Ribeye/CtBP2 staining became shorter and less defined, with dispersed immunoreactive puncta of variable size and less intensity in the *miR-183C*$^{GT/GT}$ retina as early as age 5 wk (Fig. 7 *A*, *B*, *E*, and *F*), suggesting early-onset abnormalities of synaptic ribbons. This difference became more striking in 1-y-old animals (Fig. 7 *C* and *D*), suggesting the progression of synaptic defects. Consistently, peanut agglutinin (PNA) staining, which labels the inner and outer segment as well as pedicles of cone photoreceptors (53), showed that the number and size of cone pedicles apparently were decreased in 5-wk-old *miR-183C*$^{GT/GT}$ mice (Fig. 7 *E* and *F*) and were reduced further in 1-y-old mice (*SI Appendix*, Fig. S18), suggesting defects in the maturation of photoreceptor termini.

To evaluate the photoreceptor synaptic structures directly, we performed EM of the retinas of 5-wk-old mice. Consistent with Ribeye/CtBP2 IF data, EM showed that, although synaptic ribbons were developed, ribbon size was decreased significantly in the *miR-183C*$^{GT/GT}$ mice as compared with their wild-type littermates (Fig. 7 *G*–*J*).

Taken together, these observations support the notion that members of *miR-183/96/182* modulate synaptic connections of photoreceptors to downstream neurons by directly and indirectly regulating a wide range of molecules involved in synaptogenesis and synaptic transmissions, contributing to retinal functional defects of *miR-183C*$^{GT/GT}$ mice (see Fig. 9).

Inactivation of the *miR-183/96/182* Gene Disrupts Normal Expression of Photoreceptor Genes and Postnatal Development of Photoreceptors, Contributing to Retinal Degeneration. Among the genes with abnormal expression are some known to be important in the pho-

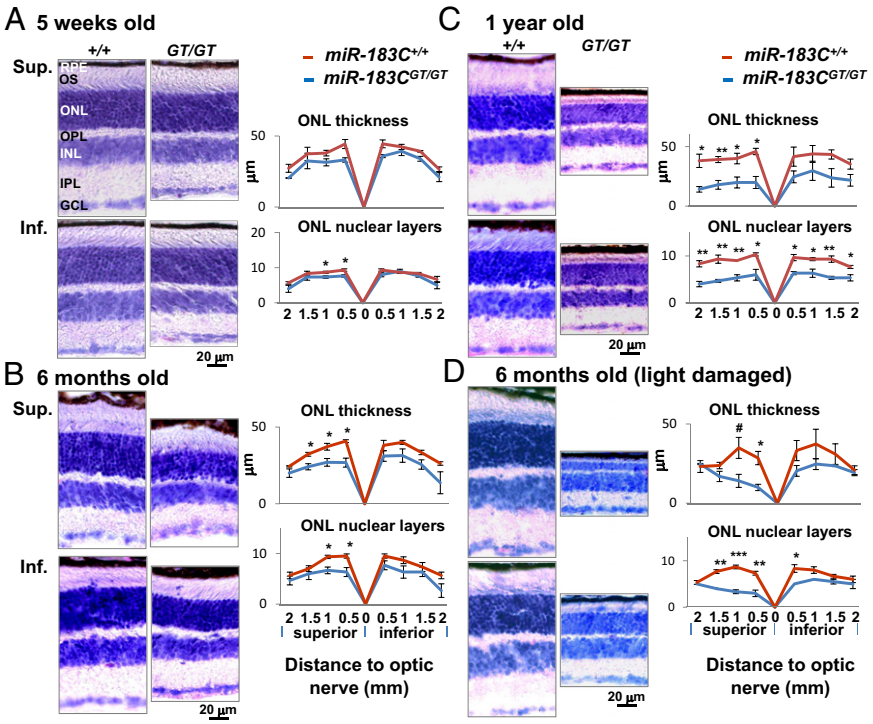

Fig. 6. Inactivation of the *miR-183/96/182* gene resulted in progressive retinal degeneration and increased susceptibility to light damage. (*A*–*C*) (*Left*) H&E staining of sagittal sections of the retina of 5-wk- (*A*), 6-mo- (*B*), and 1-y-old (*C*) *miR-183C*$^{GT/GT}$ and wild-type littermate control mice (*miR-183C*$^{+/+}$). (*Right*) Measurements of the thickness the ONL (*Upper*) and the number of nuclear layers of the ONL at different locations in reference to the optic nerve (*Lower*). Sup, superior; Inf, inferior. (*D*) H&E staining (*Left*) and measurement (*Right*) of the retina of 6-mo-old *miR-183C*$^{GT/GT}$ and wild-type littermate control mice 2 wk after a 2-h exposure to bright light. $^{\#}P < 0.06$; $^{*}P < 0.05$; $^{**}P < 0.01$; $^{***}P < 0.001$.

totransduction pathway and to be responsible for retinal diseases (*SI Appendix*, Table S9). By qRT-PCR analysis, we confirmed reduced expression of M-cone opsin, *Opn1mw*, and cone-specific arrestin, *Arr3*, by 2.54- and 2.74-fold, respectively (*SI Appendix*, Table S9; see also *SI Appendix*, Table S11*B*). IF of whole-mount retina and retinal sections validated that *Opn1mw* was decreased in the retina of 5-wk-old *miR-183C*$^{GT/GT}$ mice (Fig. 8 *A* and *B*). Quantification of M opsin- and PNA-positive cones in the whole-mount retina showed that both the total number and the percentage of M opsin-positive cones in total cones (PNA-positive) were decreased significantly in the superior retina, by 49% and 26%, respectively (Fig. 8*A*), whereas no significant changes were seen in the total number of cones or the number of M opsin–positive cones in the inferior retina. At age 1 y M opsin was almost completely lost in *miR-183C*$^{GT/GT}$ retina (Fig. 8*C*). These data suggest that M opsin-positive cones were the most affected photoreceptors in *miR-183C*$^{GT/GT}$ mice and that this increased functional vulnerability of M opsin-positive cones leads to more severe and faster-progressing defects in photopic ERGs (Fig. 5) and to the uneven distribution of retinal degeneration in *miR-183C*$^{GT/GT}$ mice (Fig. 6).

Inactivation of the *miR-183/96/182* Gene Also Results in Vestibular Dysfunction. In addition to retinal defects, *miR-183C*$^{GT/GT}$ mice exhibit circling behavior and an unstable gait (Movies S1 and S2). These phenotypic features are typical of defects in vestibular organs (54) and appeared as early as 4 wk of age. Because *miR-183/96/182* is highly expressed in the vestibular organs (Fig. 4 *A* and *C*), this phenotype likely indicates defects in the vestibular organ and possibly in other sensory organs. In the current work we have focused on the retina.

Discussion

We have shown that the *miR-183/96/182* cluster is located in an intron of a three-exon gene that spans more than 15 kb on mouse Chr6qA3.3. The transcription start site of the *miR-183/96/182* gene is about 4.4 kb upstream of *premiR-183* (Fig. 1*B*). This location was consistent with predictions by genomic and epigenomic signatures for active promoters (55, 56). There are two possible transcripts (I and II) differing by alternative utilization of the second exon with the *miR-183/96/182* cluster residing in intron 1. Transcript II has four possible ORFs, encoding putative peptides of 63–98 aa, suggesting that the *miR-183/96/182* gene is potentially a protein-coding gene. Proteomic studies will be required to determine if any of these peptides actually are produced.

We characterized a gene-trap ES clone, D016D06, in which the gene-trap construct was inserted downstream of Ex1 in the intron of the *miR-183/96/182* gene (Fig. 1*C*), and we used this cell line to produce a mouse model, the *miR-183C*$^{GT/GT}$ mouse, in which the *miR-183/96/182* gene was inactivated (Fig. 2). In qRT-PCR analysis, low levels of expression (<34% of wild-type control) of members of the *miR-183/96/182* cluster were detected in the OE (Fig. 2*G*). This expression may be a result of nonspecific amplification; however, we cannot exclude the possibility that alternative promoter(s) 3′ to the gene-trap insertion site may have resulted in leaky expression of the cluster in the OE.

Using X-Gal staining, we confirmed that the β-geo cassette in the gene-trap allele, *miR-183C*^{GT}, followed endogenous expression patterns of the cluster developmentally, spatially, and temporally in all major sensory organs (Figs. 3 and 4 and *SI Appendix*, Figs. S11–S13), providing a powerful expression-tracing marker for the *miR-183/96/182* gene. We also identified expression in the VNO (Fig. 4*B*) and pineal body (Fig. 4*C* and *SI Appendix*, Fig. S14), expanding the known expression domains of *miR-183/96/182* gene.

We demonstrated that inactivation of the *miR-183/96/182* gene in *miR-183C*$^{GT/GT}$ mice results in abnormalities of both scotopic and photopic ERGs, with decreased *b*-wave amplitudes as the most prominent defect (Fig. 5 and *SI Appendix*, Fig. S15). The ERG *b* wave reflects activities of depolarizing bipolar cells (36–39). Because, in retina, *miR-183/96/182* is expressed predominantly in photoreceptors, our results suggest that the decreased *b*-wave amplitude in *miR-183C*$^{GT/GT}$ mice is a consequence of impaired synaptic transmission of photoreceptors. The defects in *b*-wave amplitude were detected as early as age 5 wk, the earliest time tested (Fig. 5), suggesting that, in *miR-183C*$^{GT/GT}$ mice, functional synaptic connections between photoreceptors and downstream bipolar cells are not properly established.

This model is supported by our gene-expression analysis on the retina of *miR-183C*$^{GT/GT}$ mice. We found that the genes with significantly altered expression included those involved in

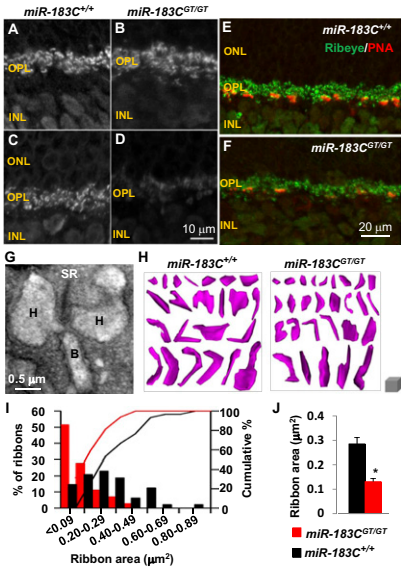

Fig. 7. Inactivation of the *miR-183/96/182* gene resulted in morphological and molecular changes in the synaptic ribbons of photoreceptors in *miR-183C*$^{GT/GT}$ mice. (*A–D*) Confocal images of Ribeye IF in the retinas of 5-wk- (*A* and *B*) and 1-y-old (*C* and *D*) *miR-183C*$^{GT/GT}$ mice (*B* and *D*) and their wild-type littermate controls (*A* and *C*). (*E* and *F*) Coimmunostaining of Ribeye (green) and PNA (red) in retinas of 5-wk-old *miR-183C*$^{GT/GT}$ mice (*F*) and their wild-type littermate controls (*E*). (*G*) An electron micrograph of a ribbon synapse of an *miR-183C*$^{+/+}$ mouse, showing a typical triad configuration of photoreceptor ribbon synapse. SR, synaptic ribbon; H, horizontal cell; B, bipolar cell. (*H*) Example of a 3D reconstruction of synaptic ribbons in the OPL of *miR-183C*$^{GT/GT}$ mice (n = 2) and their wild-type littermates (*miR-183C*$^{+/+}$ mice, n = 2), respectively. (Scale cube, 500 nm^3.) (*I* and *J*) Distribution of synaptic ribbons by size (*I*) and mean ribbon areas of *miR-183C*$^{GT/GT}$ (red; n = 72) and *miR-183C*$^{+/+}$ littermate controls (black; n = 49) (*J*). Data are shown as mean ± SEM; *$P < 0.01$.

synaptogenesis, synaptic contact, and transmission of nerve impulses (*SI Appendix*, Table S7). Using qRT-PCR, we confirmed the differences in expression of glutamate transporter, solute carrier family 1, member 1 (*Slc1a1*) (~1.9-fold increase) (20, 57–59), acetylcholinesterase (*AChE*) (~1.4-fold increase) (60, 61), cholinergic receptor nicotinic beta polypeptide 1 (*Chrnb1*) (2.0-fold increase) (62), Cortactin (*Cttn*) (~1.4-fold increase) (63–67), EphB receptor tyrosine kinase, Eph receptor B3 (*Ephb3*) (~1.6-fold increase) (68–71), Syndecan 2 (*Sdc2*) (~1.6-fold increase) (72–74), vesicle-associated membrane protein 8 (*VAMP8*) (~1.8-fold increase) (75–80), presenilin 2 (*Psen2*) (81–86) (~1.5-fold increase), and calcium channel, voltage-dependent, alpha 2/delta subunit 3 (*Cacna2d3*) (~1.7-fold decrease) (39, 87–90) (*SI Appendix*, Tables S7, S10, and S11). *Slc1a1*, *Cttn*, *Chrnb1*, and *Psen2* are experimentally confirmed and/or predicted targets for members of *miR-183/96/182* (20, 91) (*SI Appendix*, Table S7*B*), suggesting that *miR-183/96/182* directly regulates the expression of these genes.

Our gene-expression analysis also revealed that expression of genes encoding key components of both classical complement system and MHCI molecules, including *C1qc* and *C4B*, *H2-K1*, and *B2M*, were increased significantly in the retina of *miR-183C*$^{GT/GT}$ mice, by 1.5–1.7 fold (*SI Appendix*, Table S8), suggesting that activation of the complement system and dysregulation of MHCI molecules contribute to defects of synaptic connectivity in the retina of *miR-183C*$^{GT/GT}$ mice. The classical complement cascade recently has been shown to play important roles in selective elimination of inappropriate synapses during a discrete window of postnatal development of the visual system (43). Aberrant expression of *C1q* in synapses of adult retina is suggested to contribute to synapse loss in glaucoma mice (43). MHCI molecules, components of the adaptive immune system, also are shown to participate in activity-dependent synaptic remodeling (45–49).

Our hypothesis that abnormal photoreceptor synaptic connection is the primary defect in the mutant retina was proved further by IF and EM studies. PNA staining revealed decreased number and size of cone pedicles in the outer plexiform layer (OPL), suggesting defects in photoreceptor terminal development (Fig. 7 *E* and *F*). Ribeye/CtBP2 IF (Fig. 7 *A–F*) and EM (Fig. 7 *G–J*) consistently demonstrated that the size of synaptic ribbons was decreased significantly in the *miR-183C*$^{GT/GT}$ mice as early as age 5 wk. These defects worsened with age in 1-y-old mice (Fig. 7 *C* and *D* and *SI Appendix*, Fig. S18).

The synaptic defect of the retina of *miR-183C*$^{GT/GT}$ mice is consistent with IE abnormalities of *miR-96* mutants (22, 23), in which there is arrest of hair cell development around P0; remodeling of the auditory nerve synaptic connections within the cochlea fails to occur (24). These results suggest that defining functional synaptic connections may be a conserved function of the *miR-183/96/182* cluster in sensory organs.

Mouse retina has dichromatic color vision, with cones expressing two opsin photopigments sensitive to short (S-opsin) or middle (M opsin) wavelengths (92). The expression of cone opsins follows distinct temporal and spatial controls. S-opsin is more concentrated in the inferior retina, and M opsin is expressed predominantly in the

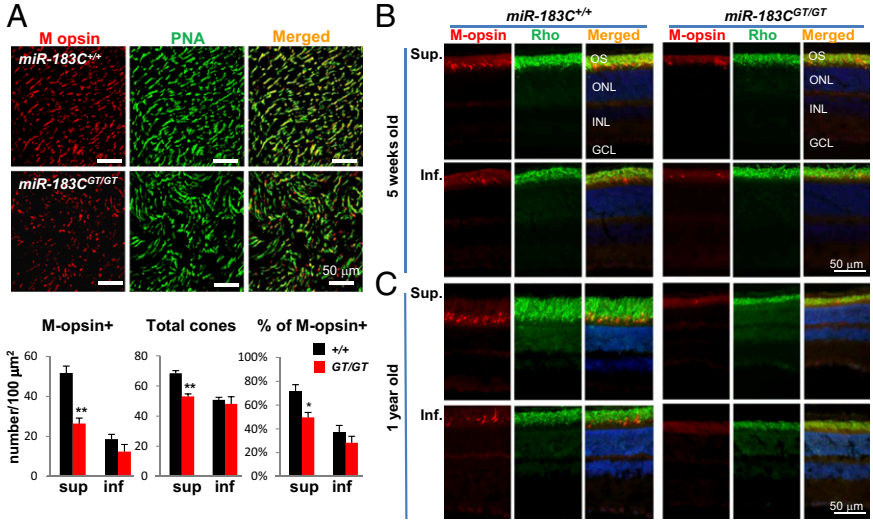

Fig. 8. Inactivation of the *miR-183/96/182* gene resulted in a significant decrease of M opsin expression in the retina. PNA staining and co-IF of whole-mount retina (*A*) and retinal sections (*B* and *C*) of 5-wk- (*A* and *B*) and 1-y-old (*C*) *miR-183C*$^{GT/GT}$ mice and their wild-type (*miR-183C*$^{+/+}$) littermate controls. The histograms at the bottom of *A* show the number of M opsin–positive (M opsin+) cones, the total number of cones per square micrometer, and the percentage of total cones that were M opsin positive in the superior (sup.) and inferior (inf.) retina.

superior cones (93, 94). Developmentally, M opsin is induced in the second postnatal week and is the last of all the opsins in photoreceptors to be expressed (95, 96). In retina, the *miR-183/96/182* cluster expression increases significantly only after birth (8); therefore, these miRNAs function mostly in the postnatal retina. Inactivation of the cluster may have the greatest impact on the expression of the last-expressed M opsin. Our microarray profiling and qRT-PCR (*SI Appendix*, Tables S9 and S11*B*) showed that M opsin expression was decreased significantly, by ∼2.5-fold, in 5-wk-old *miR-183C*$^{GT/GT}$ mice. The total number and the percentage of M opsin–positive cones were decreased significantly in *miR-183C*$^{GT/GT}$ mice (Fig. 8*A*), suggesting that some cones were generated but failed to express M opsin. Our result also showed that the total number of cones was slightly decreased in the superior retina (22%) (Fig. 8*A*), possibly as the result of either decreased production or degeneration. Nevertheless, decreased expression of M opsin may affect the overall competence and survival of M opsin-positive cones, resulting in the greater degeneration in the superior retina than in the inferior retina (Fig. 6 *B* and *C*), the greater sensitivity to light damage (Fig. 6*D*), and the more severe photopic ERG abnormalities than scotopic ERG seen in *miR-183C*$^{GT/GT}$ mice (Fig. 5).

In addition to M opsin, our gene-expression profiling revealed that many other genes involved in the phototransduction pathway and photoreceptor morphogenesis are dysregulated modestly (by ∼1.2–2.3 fold) (*SI Appendix*, Table S9). Rora, a key transcription factor, which normally is expressed in cones from P3 and is required for cone expression of opsin (97), is decreased modestly (by ∼1.3 fold) in the retina of *miR-183C*$^{GT/GT}$ mice (*SI Appendix*, Table S9*A*), possibly contributing to decreased expression of M opsin. Another key transcription factor, Nrl, which regulates many photoreceptor-specific genes and the terminal differentiation of rod photoreceptors (98–103), is reduced slightly (by ∼1.2 fold) in the retina of *miR-183C*$^{GT/GT}$ mice (*SI Appendix*, Table S9). Decreased expression of these key transcription factors may contribute to secondary decreased expression of a wide range of photoreceptor-specific genes. Additional proteomic studies on gene-expression changes at protein levels in the retina will provide deeper insight into their impact on retinal defects of *miR-183C*$^{GT/GT}$ mice.

Although ERG *a* waves did not show significant changes initially in 5-wk-old *miR-183C*$^{GT/GT}$ mice (Fig. 5), there may be subtle functional changes in individual photoreceptors; because ERGs represent the combined electrical activity of different cells in the retina, subtle changes in individual photoreceptors may not be fully detected. Single-cell recording of rod and cone photoreceptors (104) using different wave-length stimuli may differentiate early subtle functional changes of different photoreceptors in *miR-183C*$^{GT/GT}$ mice.

The *miR-183C*$^{GT/GT}$ mouse is a model of the complete inactivation of the cluster gene. The 3p miRNAs are expressed at much lower levels than the predominantly expressed *miR-183*, *miR-96*, and *miR-182* (*SI Appendix*, Fig. S9), and whether the putative peptides encoded by transcript II (Fig. 1*B*) are translated in vivo still needs to be determined. We could not exclude the possibility that the 3p miRNAs, the two transcripts, and their putative peptides had physiological functions in vivo. Consequently, phenotypes and gene-expression changes in *miR-183C*$^{GT/GT}$ mice must be considered as a result of a combined loss of all products of the cluster gene. Therefore, our *miR-183C*$^{GT/GT}$ mouse model provides insights into the overall functions of the cluster gene. However, the exact functions of each product of the cluster gene are yet to be defined. A "clean" knockout of the miRNA cluster without disruption of the transcripts will help determine whether these phenotypes are a result of the loss of the miRNAs of the cluster. Transgenes of individual products or combinations of individual products of the cluster gene in *miR-183C*$^{GT/GT}$ mice will help dissect the functions of each component of the cluster gene and/or its contribution to the phenotypes and gene-expression changes in *miR-183C*$^{GT/GT}$ mice. Therefore, our *miR-183C*$^{GT/GT}$ mouse model provides an important tool for studying the functions of individual products of the *miR-183/96/182* gene in all sensory organs.

In mouse, both rod and cone photoreceptor differentiation and synaptogenesis occur postnatally, starting at P4–5 (105), coincident with developmental up-regulation of *miR-183/96/182* (Fig. 3*F*). Our data suggest that the *miR-183/96/182* gene plays important roles in postnatal functional photoreceptor differentiation by directly and indirectly regulating the expression of genes important for synaptogenesis and synaptic function, photoreceptor morphogenesis, and phototransduction pathway. Inactivation of the cluster disrupts the homeostasis and function of the photoreceptors, leading to progressive degeneration of the retina (Fig. 9). The ERG abnormalities in these mice resemble those observed in human incomplete stationary congenital night blindness (106) and in the mouse mutants lacking *b* waves (39). Although not yet fully characterized, the prominent vestibular dysfunction of *miR-183C*$^{GT/GT}$ mice suggests defects in the IE and possibly in other sensory organs. Thus, these animals exhibit a sensory syndrome clinically reminiscent of Usher syndrome (107). However, retinal defects in Usher syndrome are manifested as retinitis pigmentosa, with rod photoreceptors primarily affected initially (107), whereas in *miR-183C*$^{GT/GT}$ mice the functions of photoreceptors were relatively normal initially, and cone photoreceptors were most vulnerable to degeneration. Although the phenotypes and molecular changes in *miR-183C*$^{GT/GT}$ mice are not a perfect match for any known human disease, patients with mutation-negative Usher-like syndrome would be good candidates for *miR-183/96/182* loss-of-function mutations. Studies on genetic variation or polymorphisms around the *miR-183/96/182* gene are warranted in patients with age-related, progressive retinal and/or multiple sensory defects and other neurological conditions.

Materials and Methods

Gene-Trap Cell Line and Mouse Production. Gene-trap ESC clone D016D06, was obtained from the German Gene Trap Consortium (http://tikus.gsf.de/). Standard protocols of ESC culture were followed as described previously (108). Chimeric mice were produced at the Transgenic Core Facility of the University of Illinois at Chicago using standard protocols (109). See *SI Appendix* for more details of ESC characterization and mouse production. Mice were kept in 12-h light (<100 lx)12-h dark cycles with light on at 7:00 AM [zeitgeber time (ZT) 0] and off at 7:00 PM (ZT12). Animal care and husbandry followed National Institute of Health (NIH) and Association for Research in Vision and Ophthalmology (ARVO) guidelines. All protocols were approved by the Institutional Animal Care and Use Committee of Rush University Medical Center.

RNA Isolation and Northern Blot Analysis. Protocols for RNA isolation and Northern blot analysis as described previously (8) were followed with modifications. See *SI Appendix* for more details.

ERG. ERGs were carried out using a portable hmsERG machine (OccuScience). For scotopic ERG, we followed a protocol similar to that we described previously

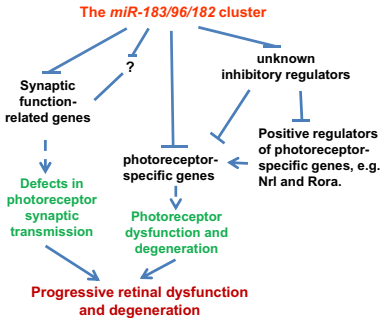

Fig. 9. Hypothetical model of in vivo functions of the *miR-183/96/182* gene in the retina. Members of *miR-183/96/182* directly and indirectly regulate multiple genes involved in photoreceptor maturation and synaptic connections with downstream bipolar cells. When the *miR-183/96/182* gene is inactivated, the homeostasis of the photoreceptors is disrupted, resulting in defects in photoreceptors and their synaptic transmission, leading to progressive retinal dysfunction and degeneration.

(110), with modifications. For photopic ERGs, a protocol similar to that previously described (111) was followed. See *SI Appendix* for more details.

Preparation of Cryoprotected Sections of Adult and Embryonic Mouse Retina. A protocol similar to that described previously was followed (108). To collect embryonic retinas, we checked vaginal plugs in the females in the breeding cages every morning. When a female was plugged, we separated her from the male, recorded the date of plugging, and registered the predicted age of the embryo as 0.5 d postconception (d.p.c). We harvested the eyes at E14.5 and E16.6 and at 18.5 d.p.c. For postnatal age, we designated the day of birth as P1.

H&E Staining and Measurement of Retinal Layers. Standard H&E staining was performed as described previously (108). Retinal thickness was measured using NIS-Elements BR software on a Nikon Eclipse 80i microscope. Moving outwards from the optic nerve, measurements of the OS, ONL, OPL, INL, and IPL were taken every 500 μm on live color images; the number of nuclear layers across the ONL also was counted. Statistical analysis was performed using two-tailed *t* tests.

X-Gal Staining. X-Gal staining was performed as described previously (108). See *SI Appendix* for more details.

Antibodies, IF, and PNA Staining. Antibodies against rhodopsin (Ab5417; AbCam), M opsin (AB5405; Millipore), S-opsin (AB5407; Millipore), Ribeye/CtBP2 (612044; BD Bioscience), PSD95 (75-028; Antibody Inc.), and synaptophysin (MAB5258; Millipore) were used as primary antibodies. Alexa Fluor-conjugated secondary antibodies were purchased from Invitrogen. IF was performed as described previously (112). Fluorescein and rhodamine-conjugated PNA was purchased from Vector Laboratories. For PNA staining on retinal sections, PNA (200 μg/mL) was incubated with sections for 1 h at room temperature followed by a 10-min postfixation. For whole-mount retinal IF, a protocol similar to that previously described (113) was followed. For quantification of cones in whole-mount retina, a protocol previously described by Ng et al. (95) was followed. See *SI Appendix* for more details.

EM. Eye cups were fixed in 3% paraformaldehyde, 2.5% glutaraldehyde in 0.1 M phosphate buffer (pH 7.4) for 2 h at room temperature and then were processed for conventional EM as previously described (114). See *SI Appendix* for more details.

Gene-Expression Profiling, Data Analysis, and Confirmation Study. GeneChip Mouse Genome 430A_2 Array (Affymetrix) was used for gene-expression profiling. The probe labeling, GeneChip hybridization, and data collection were performed at the Core Facility of Research Resource Center at the University of Illinois, Chicago. See *SI Appendix* for more details.

Light-Damage Experiment. Mice were dark adapted overnight before the light-damage experiment. Pupils were dilated using 1% tropicamide solution and 2.5% phenylephrine (Bausch & Lomb) for 15 min. Then mice were exposed for 2 h to 10,000-lx cool, white fluorescent light in cages lined with aluminum foil. After light exposure mice were kept in the dark for 2 wk before being killed for preparation of retinal sections.

ACKNOWLEDGMENTS. We thank Dr. Jeremy Nathans for his comments on the manuscript and Dr. Yanshu Wang for technical consultation on PNA staining and whole-mount retinal IF. This work was supported by a grant from the Lincy Foundation (to S.X.).

1. Ambros V (2004) The functions of animal microRNAs. *Nature* 431(7006):350–355.
2. Bartel DP (2004) MicroRNAs: Genomics, biogenesis, mechanism, and function. *Cell* 116(2):281–297.
3. Wightman B, Ha I, Ruvkun G (1993) Posttranscriptional regulation of the heterochronic gene lin-14 by lin-4 mediates temporal pattern formation in C. elegans. *Cell* 75(5):855–862.
4. Lee RC, Feinbaum RL, Ambros V (1993) The C. elegans heterochronic gene lin-4 encodes small RNAs with antisense complementarity to lin-14. *Cell* 75(5):843–854.
5. Ryan DG, Oliveira-Fernandes M, Lavker RM (2006) MicroRNAs of the mammalian eye display distinct and overlapping tissue specificity. *Mol Vis* 12:1175–1184.
6. Li X, Carthew RW (2005) A microRNA mediates EGF receptor signaling and promotes photoreceptor differentiation in the Drosophila eye. *Cell* 123(7):1267–1277.
7. Wienholds E, et al. (2005) MicroRNA expression in zebrafish embryonic development. *Science* 309(5732):310–311.
8. Xu S, Witmer PD, Lumayag S, Kovacs B, Valle D (2007) MicroRNA (miRNA) transcriptome of mouse retina and identification of a sensory organ-specific miRNA cluster. *J Biol Chem* 282(34):25053–25066.
9. Xu S (2009) microRNA expression in the eyes and their significance in relation to functions. *Prog Retin Eye Res* 28(2):87–116.
10. Karali M, Peluso I, Marigo V, Banfi S (2007) Identification and characterization of microRNAs expressed in the mouse eye. *Invest Ophthalmol Vis Sci* 48(2):509–515.
11. Arora A, McKay GJ, Simpson DA (2007) Prediction and verification of miRNA expression in human and rat retinas. *Invest Ophthalmol Vis Sci* 48(9):3962–3967.
12. Hackler L, Jr., Wan J, Swaroop A, Qian J, Zack DJ (2010) MicroRNA profile of the developing mouse retina. *Invest Ophthalmol Vis Sci* 51(4):1823–1831.
13. Loscher CJ, et al. (2007) Altered retinal microRNA expression profile in a mouse model of retinitis pigmentosa. *Genome Biol* 8(11):R248.
14. Loscher CJ, et al. (2008) A common microRNA signature in mouse models of retinal degeneration. *Exp Eye Res* 87(6):529–534.
15. Lee YS, et al. (2004) Distinct roles for Drosophila Dicer-1 and Dicer-2 in the siRNA/miRNA silencing pathways. *Cell* 117(1):69–81.
16. Pinter R, Hindges R (2010) Perturbations of microRNA function in mouse dicer mutants produce retinal defects and lead to aberrant axon pathfinding at the optic chiasm. *PLoS ONE* 5(4):e10021.
17. Davis N, Mor E, Ashery-Padan R (2011) Roles for Dicer1 in the patterning and differentiation of the optic cup neuroepithelium. *Development* 138(1):127–138.
18. Georgi SA, Reh TA (2010) Dicer is required for the transition from early to late progenitor state in the developing mouse retina. *J Neurosci* 30(11):4048–4061.
19. Damiani D, et al. (2008) Dicer inactivation leads to progressive functional and structural degeneration of the mouse retina. *J Neurosci* 28(19):4878–4887.
20. Krol J, et al. (2010) Characterizing light-regulated retinal microRNAs reveals rapid turnover as a common property of neuronal microRNAs. *Cell* 141(4):618–631.
21. Jin ZB, et al. (2009) Targeted deletion of miR-182, an abundant retinal microRNA. *Mol Vis* 15:523–533.
22. Mencía A, et al. (2009) Mutations in the seed region of human miR-96 are responsible for nonsyndromic progressive hearing loss. *Nat Genet* 41(5):609–613.
23. Lewis MA, et al. (2009) An ENU-induced mutation of miR-96 associated with progressive hearing loss in mice. *Nat Genet* 41(5):614–618.
24. Kuhn S, et al. (2011) miR-96 regulates the progression of differentiation in mammalian cochlear inner and outer hair cells. *Proc Natl Acad Sci USA* 108(6):2355–2360.
25. Li H, Kloosterman W, Fekete DM (2010) MicroRNA-183 family members regulate sensorineural fates in the inner ear. *J Neurosci* 30(9):3254–3263.
26. Zhu Q, et al. (2011) Sponge transgenic mouse model reveals important roles for the microRNA-183 (miR-183)/96/182 cluster in postmitotic photoreceptors of the retina. *J Biol Chem* 286(36):31749–31760.
27. Stanford WL, Cohn JB, Cordes SP (2001) Gene-trap mutagenesis: Past, present and beyond. *Nat Rev Genet* 2(10):756–768.
28. Hansen J, et al. (2003) A large-scale, gene-driven mutagenesis approach for the functional analysis of the mouse genome. *Proc Natl Acad Sci USA* 100(17):9918–9922.
29. Schnütgen F, et al. (2005) Genomewide production of multipurpose alleles for the functional analysis of the mouse genome. *Proc Natl Acad Sci USA* 102(20):7221–7226.
30. Friedrich G, Soriano P (1991) Promoter traps in embryonic stem cells: A genetic screen to identify and mutate developmental genes in mice. *Genes Dev* 5(9):1513–1523.
31. Antoch MP, et al. (1997) Functional identification of the mouse circadian Clock gene by transgenic BAC rescue. *Cell* 89(4):655–667.
32. King DP, et al. (1997) Positional cloning of the mouse circadian clock gene. *Cell* 89(4):641–653.
33. Hastings MH, Herzog ED (2004) Clock genes, oscillators, and cellular networks in the suprachiasmatic nuclei. *J Biol Rhythms* 19(5):400–413.
34. Lolley RN, Craft CM, Lee RH (1992) Photoreceptors of the retina and pinealocytes of the pineal gland share common components of signal transduction. *Neurochem Res* 17(1):81–89.
35. Blackshaw S, Snyder SH (1997) Developmental expression pattern of phototransduction components in mammalian pineal implies a light-sensing function. *J Neurosci* 17(21):8074–8082.
36. Robson JG, Frishman LJ (1995) Response linearity and kinetics of the cat retina: The bipolar cell component of the dark-adapted electroretinogram. *Vis Neurosci* 12(5):837–850.
37. Stockton RA, Slaughter MM (1989) B-wave of the electroretinogram. A reflection of ON bipolar cell activity. *J Gen Physiol* 93(1):101–122.
38. Hood DC, Birch DG (1996) Beta wave of the scotopic (rod) electroretinogram as a measure of the activity of human on-bipolar cells. *J Opt Soc Am A Opt Image Sci Vis* 13(3):623–633.
39. McCall MA, Gregg RG (2008) Comparisons of structural and functional abnormalities in mouse b-wave mutants. *J Physiol* 586(Pt 18):4385–4392.
40. Penn RD, Hagins WA (1969) Signal transmission along retinal rods and the origin of the electroretinographic a-wave. *Nature* 223(5202):201–204.
41. Peachey NS, Goto Y, Quiambao AB, al-Ubaidi MR (1995) Functional consequences of oncogene-induced photoreceptor degeneration in transgenic mice. *Vis Neurosci* 12(3):513–522.
42. Lyubarsky AL, Pugh EN, Jr. (1996) Recovery phase of the murine rod photoresponse reconstructed from electroretinographic recordings. *J Neurosci* 16(2):563–571.
43. Stevens B, et al. (2007) The classical complement cascade mediates CNS synapse elimination. *Cell* 131(6):1164–1178.
44. Perry VH, O'Connor V (2008) C1q: The perfect complement for a synaptic feast? *Nat Rev Neurosci* 9(11):807–811.

45. Corriveau RA, Huh GS, Shatz CJ (1998) Regulation of class I MHC gene expression in the developing and mature CNS by neural activity. *Neuron* 21(3):505–520.
46. Huh GS, et al. (2000) Functional requirement for class I MHC in CNS development and plasticity. *Science* 290(5499):2155–2159.
47. Shatz CJ (2009) MHC class I: An unexpected role in neuronal plasticity. *Neuron* 64(1): 40–45.
48. Boulanger LM (2009) Immune proteins in brain development and synaptic plasticity. *Neuron* 64(1):93–109.
49. Datwani A, et al. (2009) Classical MHCI molecules regulate retinogeniculate refinement and limit ocular dominance plasticity. *Neuron* 64(4):463–470.
50. Dowling JE, Boycott BB (1966) Organization of the primate retina: Electron microscopy. *Proc R Soc Lond B Biol Sci* 166(2):80–111.
51. Cohen AI (1960) The ultrastructure of the rods of the mouse retina. *Am J Anat* 107: 23–48.
52. Schmitz F, Königstorfer A, Südhof TC (2000) RIBEYE, a component of synaptic ribbons: A protein's journey through evolution provides insight into synaptic ribbon function. *Neuron* 28(3):857–872.
53. Blanks JC, Johnson LV (1984) Specific binding of peanut lectin to a class of retinal photoreceptor cells. A species comparison. *Invest Ophthalmol Vis Sci* 25(5):546–557.
54. Wenngren BI, Anniko M (1989) Vestibular hair cell pathology in the dancer mouse mutant. *Acta Otolaryngol* 107(3-4):182–190.
55. Marson A, et al. (2008) Connecting microRNA genes to the core transcriptional regulatory circuitry of embryonic stem cells. *Cell* 134(3):521–533.
56. Ozsolak F, et al. (2008) Chromatin structure analyses identify miRNA promoters. *Genes Dev* 22(22):3172–3183.
57. Copenhagen DR, Jahr CE (1989) Release of endogenous excitatory amino acids from turtle photoreceptors. *Nature* 341(6242):536–539.
58. Gaal L, et al. (1998) Postsynaptic response kinetics are controlled by a glutamate transporter at cone photoreceptors. *J Neurophysiol* 79(1):190–196.
59. Hasegawa J, Obara T, Tanaka K, Tachibana M (2006) High-density presynaptic transporters are required for glutamate removal from the first visual synapse. *Neuron* 50(1):63–74.
60. Zimmerman G, Soreq H (2006) Termination and beyond: Acetylcholinesterase as a modulator of synaptic transmission. *Cell Tissue Res* 326(2):655–669.
61. Grisaru D, Sternfeld M, Eldor A, Glick D, Soreq H (1999) Structural roles of acetylcholinesterase variants in biology and pathology. *Eur J Biochem* 264(3):672–686.
62. Friese MB, Blagden CS, Burden SJ (2007) Synaptic differentiation is defective in mice lacking acetylcholine receptor beta-subunit tyrosine phosphorylation. *Development* 134(23):4167–4176.
63. Cao H, Chen J, Krueger EW, McNiven MA (2010) SRC-mediated phosphorylation of dynamin and cortactin regulates the "constitutive" endocytosis of transferrin. *Mol Cell Biol* 30(3):781–792.
64. Kruchten AE, Krueger EW, Wang Y, McNiven MA (2008) Distinct phospho-forms of cortactin differentially regulate actin polymerization and focal adhesions. *Am J Physiol Cell Physiol* 295(5):C1113–C1122.
65. Krueger EW, Orth JD, Cao H, McNiven MA (2003) A dynamin-cortactin-Arp2/3 complex mediates actin reorganization in growth factor-stimulated cells. *Mol Biol Cell* 14(3):1085–1096.
66. Gray NW, Kruchten AE, Chen J, McNiven MA (2005) A dynamin-3 spliced variant modulates the actin/cortactin-dependent morphogenesis of dendritic spines. *J Cell Sci* 118(Pt 6):1279–1290.
67. Knöll B, Drescher U (2004) Src family kinases are involved in EphA receptor-mediated retinal axon guidance. *J Neurosci* 24(28):6248–6257.
68. Hindges R, McLaughlin T, Genoud N, Henkemeyer M, O'Leary DD (2002) EphB forward signaling controls directional branch extension and arborization required for dorsal-ventral retinotopic mapping. *Neuron* 35(3):475–487.
69. Liu X, Hawkes E, Ishimaru T, Tran T, Sretavan DW (2006) EphB3: An endogenous mediator of adult axonal plasticity and regrowth after CNS injury. *J Neurosci* 26(12):3087–3101.
70. Ciossek T, et al. (1998) Eph receptor-ligand interactions are necessary for guidance of retinal ganglion cell axons in vitro. *Eur J Neurosci* 10(5):1574–1580.
71. Fu CT, Sretavan D (2012) Involvement of EphB/Ephrin-B signaling in axonal survival in mouse experimental glaucoma. *Invest Ophthalmol Vis Sci* 53(1):76–84.
72. Ethell IM, Hagihara K, Miura Y, Irie F, Yamaguchi Y (2000) Synbindin, A novel syndecan-2-binding protein in neuronal dendritic spines. *J Cell Biol* 151(1):53–68.
73. Ethell IM, Yamaguchi Y (1999) Cell surface heparan sulfate proteoglycan syndecan-2 induces the maturation of dendritic spines in rat hippocampal neurons. *J Cell Biol* 144(3):575–586.
74. Ethell IM, et al. (2001) EphB/syndecan-2 signaling in dendritic spine morphogenesis. *Neuron* 31(6):1001–1013.
75. Zeng Q, et al. (1998) A novel synaptobrevin/VAMP homologous protein (VAMP5) is increased during in vitro myogenesis and present in the plasma membrane. *Mol Biol Cell* 9(9):2423–2437.
76. Wang CC, et al. (2004) A role of VAMP8/endobrevin in regulated exocytosis of pancreatic acinar cells. *Dev Cell* 7(3):359–371.
77. Wang CC, et al. (2007) VAMP8/endobrevin as a general vesicular SNARE for regulated exocytosis of the exocrine system. *Mol Biol Cell* 18(3):1056–1063.
78. Ho YH, Cai DT, Huang D, Wang CC, Wong SH (2009) Caspases regulate VAMP-8 expression and phagocytosis in dendritic cells. *Biochem Biophys Res Commun* 387(2): 371–375.
79. Sherry DM, Wang MM, Frishman LJ (2003) Differential distribution of vesicle associated membrane protein isoforms in the mouse retina. *Mol Vis* 9:673–688.
80. Morgans CW, et al. (2009) Loss of the Synaptic Vesicle Protein SV2B results in reduced neurotransmission and altered synaptic vesicle protein expression in the retina. *PLoS ONE* 4(4):e5230.
81. De Strooper B, et al. (1999) A presenilin-1-dependent gamma-secretase-like protease mediates release of Notch intracellular domain. *Nature* 398(6727):518–522.
82. Kopan R, Ilagan MX (2004) Gamma-secretase: Proteasome of the membrane? *Nat Rev Mol Cell Biol* 5(6):499–504.
83. Sisodia SS, St George-Hyslop PH (2002) gamma-Secretase, Notch, Abeta and Alzheimer's disease: Where do the presenilins fit in? *Nat Rev Neurosci* 3(4):281–290.
84. Wang R, Tang P, Wang P, Boissy RE, Zheng H (2006) Regulation of tyrosinase trafficking and processing by presenilins: Partial loss of function by familial Alzheimer's disease mutation. *Proc Natl Acad Sci USA* 103(2):353–358.
85. Esselens C, et al. (2004) Presenilin 1 mediates the turnover of telencephalin in hippocampal neurons via an autophagic degradative pathway. *J Cell Biol* 166(7): 1041–1054.
86. Parent A, Linden DJ, Sisodia SS, Borchelt DR (1999) Synaptic transmission and hippocampal long-term potentiation in transgenic mice expressing FAD-linked presenilin 1. *Neurobiol Dis* 6(1):56–62.
87. Barnes S, Kelly ME (2002) Calcium channels at the photoreceptor synapse. *Adv Exp Med Biol* 514:465–476.
88. Strom TM, et al. (1998) An L-type calcium-channel gene mutated in incomplete X-linked congenital stationary night blindness. *Nat Genet* 19(3):260–263.
89. Bech-Hansen NT, et al. (1998) Loss-of-function mutations in a calcium-channel alpha1-subunit gene in Xp11.23 cause incomplete X-linked congenital stationary night blindness. *Nat Genet* 19(3):264–267.
90. Wycisk KA, et al. (2006) Mutation in the auxiliary calcium-channel subunit CACNA2D4 causes autosomal recessive cone dystrophy. *Am J Hum Genet* 79(5): 973–977.
91. Zhang L, Liu T, Huang Y, Liu J (2011) microRNA-182 inhibits the proliferation and invasion of human lung adenocarcinoma cells through its effect on human cortical actin-associated protein. *Int J Mol Med* 28(3):381–388.
92. Ebrey T, Koutalos Y (2001) Vertebrate photoreceptors. *Prog Retin Eye Res* 20(1): 49–94.
93. Szél A, et al. (1992) Unique topographic separation of two spectral classes of cones in the mouse retina. *J Comp Neurol* 325(3):327–342.
94. Applebury ML, et al. (2000) The murine cone photoreceptor: A single cone type expresses both S and M opsins with retinal spatial patterning. *Neuron* 27(3):513–523.
95. Ng L, et al. (2001) A thyroid hormone receptor that is required for the development of green cone photoreceptors. *Nat Genet* 27(1):94–98.
96. Fei Y (2003) Development of the cone photoreceptor mosaic in the mouse retina revealed by fluorescent cones in transgenic mice. *Mol Vis* 9:31–42.
97. Fujieda H, Bremner R, Mears AJ, Sasaki H (2009) Retinoic acid receptor-related orphan receptor alpha regulates a subset of cone genes during mouse retinal development. *J Neurochem* 108(1):91–101.
98. Swaroop A, et al. (1992) A conserved retina-specific gene encodes a basic motif/ leucine zipper domain. *Proc Natl Acad Sci USA* 89(1):266–270.
99. Mitton KP, et al. (2000) The leucine zipper of NRL interacts with the CRX homeodomain. A possible mechanism of transcriptional synergy in rhodopsin regulation. *J Biol Chem* 275(38):29794–29799.
100. Pittler SJ, et al. (2004) Functional analysis of the rod photoreceptor cGMP phosphodiesterase alpha-subunit gene promoter: Nrl and Crx are required for full transcriptional activity. *J Biol Chem* 279(19):19800–19807.
101. Yoshida S, et al. (2004) Expression profiling of the developing and mature Nrl-/- mouse retina: Identification of retinal disease candidates and transcriptional regulatory targets of Nrl. *Hum Mol Genet* 13(14):1487–1503.
102. Oh EC, et al. (2008) Rod differentiation factor NRL activates the expression of nuclear receptor NR2E3 to suppress the development of cone photoreceptors. *Brain Res* 1236:16–29.
103. Hennig AK, Peng GH, Chen S (2008) Regulation of photoreceptor gene expression by Crx-associated transcription factor network. *Brain Res* 1192:114–133.
104. Baylor DA, Lamb TD, Yau KW (1979) The membrane current of single rod outer segments. *J Physiol* 288:589–611.
105. Rich KA, Zhan Y, Blanks JC (1997) Migration and synaptogenesis of cone photoreceptors in the developing mouse retina. *J Comp Neurol* 388(1):47–63.
106. Miyake Y, Yagasaki K, Horiguchi M, Kawase Y, Kanda T (1986) Congenital stationary night blindness with negative electroretinogram. A new classification. *Arch Ophthalmol* 104(7):1013–1020.
107. Yan D, Liu XZ (2010) Genetics and pathological mechanisms of Usher syndrome. *J Hum Genet* 55(6):327–335.
108. Xu S, et al. (2004) PHR1, a PH domain-containing protein expressed in primary sensory neurons. *Mol Cell Biol* 24(20):9137–9151.
109. Nagy A, Gertsenstein M, Vintersten K, Behringer R (2003) *Manipulating the Mouse Embryo. A Laboratory Manual.* (Cold Spring Harbor Laboratory, Cold Spring Harbor, NY) 3rd Ed.
110. Perez SE, Lumayag S, Kovacs B, Mufson EJ, Xu S (2009) Beta-amyloid deposition and functional impairment in the retina of the APPswe/PS1DeltaE9 transgenic mouse model of Alzheimer's disease. *Invest Ophthalmol Vis Sci* 50(2):793–800.
111. Peachey NS, Goto Y, al-Ubaidi MR, Naash MI (1993) Properties of the mouse cone-mediated electroretinogram during light adaptation. *Neurosci Lett* 162(1-2):9–11.
112. Xu S, et al. (2007) The proliferation and expansion of retinal stem cells require functional Pax6. *Dev Biol* 304(2):713–721.
113. Ye X, et al. (2009) Norrin, frizzled-4, and Lrp5 signaling in endothelial cells controls a genetic program for retinal vascularization. *Cell* 139(2):285–298.
114. Nicholson DA, Geinisman Y (2009) Axospinous synaptic subtype-specific differences in structure, size, ionotropic receptor expression, and connectivity in apical dendritic regions of rat hippocampal CA1 pyramidal neurons. *J Comp Neurol* 512(3):399–418.
115. Young RW (1984) Cell death during differentiation of the retina in the mouse. *J Comp Neurol* 229(3):362–373.